

## **Reliability of self-sampling for accurate assessment of respiratory virus viral and immunologic kinetics**

Alpana Waghmare<sup>1,2,3</sup>, Elizabeth M. Krantz<sup>1</sup>, Subhasish Baral<sup>1</sup>, Emma Vasquez<sup>1</sup>, Tillie Loeffelholz<sup>1</sup>, E. Lisa Chung<sup>1</sup>, Urvashi Pandey<sup>1,4</sup>, Jane Kuypers<sup>5</sup>, Elizabeth R Duke<sup>1,6</sup>, Keith R. Jerome<sup>1,5</sup>, Alexander L. Greninger<sup>5</sup>, Daniel B. Reeves<sup>1</sup>, Florian Hladik<sup>1,4,6</sup>, E. Fabian Cardozo-Ojeda<sup>1</sup>, Michael Boeckh<sup>1,6,7</sup>, Joshua T. Schiffer<sup>1,6,7\*</sup>

<sup>1</sup> Vaccine and Infectious Diseases Division, Fred Hutchinson Cancer Research Center

<sup>2</sup> Department of Pediatrics, University of Washington

<sup>3</sup> Center for Clinical and Translational Research, Seattle Children's Research Institute

<sup>4</sup> Department of Obstetrics and Gynecology, University of Washington

<sup>5</sup> Department of Laboratory Medicine, University of Washington

<sup>6</sup> Department of Medicine, University of Washington

<sup>7</sup> Clinical Research Division, Fred Hutchinson Cancer Research Center

\*Corresponding author:

Joshua T. Schiffer, MD

Fred Hutchinson Cancer Research Center

1100 Fairview Ave N

Seattle, WA 98109

[jschiffe@fredhutch.org](mailto:jschiffe@fredhutch.org)

## Abstract

1  
2 The SARS-CoV-2 pandemic demonstrates the need for accurate and convenient approaches to  
3 diagnose and therapeutically monitor respiratory viral infections. We demonstrated that self-  
4 sampling with foam swabs is well-tolerated and provides quantitative viral output concordant  
5 with flocked swabs. Using longitudinal home-based self-sampling, we demonstrate nasal  
6 cytokine levels correlate and cluster according to immune cell of origin. Periods of stable viral  
7 loads are followed by rapid elimination, which could be coupled with cytokine expansion and  
8 contraction using mathematical models. Nasal foam swab self-sampling at home provides a  
9 precise, mechanistic readout of respiratory virus shedding and local immune responses.

10 The COVID-19 pandemic is an unprecedented event in modern history. As of March 30, there  
11 are 784,000 documented COVID-19 cases, which is surely an underestimation, and 37,638  
12 deaths worldwide with rapidly expanding outbreaks ongoing in dozens of countries<sup>1</sup>. Morbidity  
13 and mortality rates are dangerously high in the elderly and those with medical comorbidities<sup>2,3</sup>.  
14 Current informal estimates suggest that 20-70% of humans may become infected without global  
15 deployment of a vaccine, which is unlikely to occur in the next year. While social distancing has  
16 proven effective in several countries in Asia, these measures might not be sustainable without  
17 crippling the global economy and may not be as successfully implemented elsewhere. Under  
18 optimistic projections, social distancing may push COVID-19 to a fluctuating pattern during  
19 which periodic outbreaks necessitate repeated implementation of social distancing<sup>4</sup>. In all  
20 likelihood, this highly contagious and lethal respiratory virus will likely circulate widely for years  
21 to come<sup>5</sup>.

22  
23 A critical research priority is to develop rapid molecular tests that provide accurate diagnosis,  
24 determine infectiousness and transmissibility, and allow for monitoring of viral load during  
25 therapy<sup>6</sup>. For numerous viral infections, including influenza, viral load correlates with disease  
26 severity and secondary household attack rate<sup>7-9</sup>. Early studies suggest that peak viral load  
27 differentiates mild from severe COVID-19<sup>10</sup>. Furthermore, viral load monitoring during antiviral  
28 therapy is a mainstay for various human infections including HIV, hepatitis B, cytomegalovirus  
29 and hepatitis C infections<sup>11-17</sup>. Particularly for viruses such as SARS-CoV-2 for which severe  
30 clinical outcomes occur in a minority of patients, viral load may serve as a useful surrogate  
31 marker to design smaller, but still sufficiently powered treatment studies<sup>4,10</sup>.

32  
33 Another major unmet medical need is the ability to frequently measure the local mucosal  
34 immune response during the course of infection. It is increasingly recognized that tissue  
35 resident T-cells and antigen presenting cells are phenotypically and functionally distinct from

36 circulating immune cells, especially in the setting of respiratory viral infections<sup>18-20</sup>. Therefore,  
37 measuring immune cells in blood can fundamentally misclassify the agents responsible for viral  
38 elimination at the local level. To assess tissue resident immune cells requires biopsies which  
39 are difficult to obtain during active infection. Yet, important shifts in the immune response  
40 against respiratory viruses likely occur rapidly and in stages during the early and late phases of  
41 viral shedding<sup>21</sup>. Serial measurement of local cytokines may provide a window into the local  
42 cellular response<sup>22</sup>, but has yet to be validated from longitudinal clinical samples.

43  
44 Self-testing for respiratory viruses has been promoted for more than a decade and successfully  
45 performed both in research and primary care settings, but regulatory agencies have been slow  
46 to accept patient collected samples as valid, especially in the home setting. Recently issued  
47 initial guidelines from the United States Food and Drug Administration (FDA) required  
48 nasopharyngeal (NP) sampling using flocked swabs for diagnosis of COVID-19 by clinical  
49 laboratories<sup>23</sup>. However, as the demand for testing exponentially increases, NP swab availability  
50 significantly hampers effective and efficient testing and identification of COVID-19-infected  
51 individuals. Currently licensed flocked swabs may not be optimal for patients with vulnerable  
52 mucosal membranes and low platelet counts (e.g. following cytotoxic chemotherapy) because  
53 they are associated with some discomfort and possible bleeding. Moreover, their general level  
54 of discomfort may deter participants from collecting longitudinal samples. This may limit  
55 widespread use for self-testing, especially as surveillance testing or for use in vulnerable  
56 patients or children. Importantly, a reliable and comfortable home-based self-testing  
57 methodology is needed to prevent potentially infected individuals from entering healthcare  
58 facilities to be tested and transmitting virus to healthcare workers and other patients. Initial data  
59 on foam swabs are promising, suggesting a broader role for home-based self-swabbing for  
60 respiratory viral pandemics<sup>24,25</sup>.

61

62 Here we report data on a novel respiratory virus detection method using self-collected nasal  
63 foam swabs. This methodology expands our testing armamentarium with easily collected and  
64 comfortable swabs that can be applied to viral load and cytokine kinetic studies. Most  
65 importantly, they can be easily scaled and used at home in this time of severe testing shortages  
66 and dangerous transmission risk.

67

## 68 **Results.**

69

70 ***Concordance between foam and flocked nasal swabs for viral detection.*** Fifteen  
71 participants were enrolled within 3 days of respiratory symptom onset (**Supp Table 1**). Four  
72 participants were negative for any respiratory virus from all swabs on our multiplex PCR panel  
73 (**Table 1**). Participants swabbed each nostril with a foam swab and a flocked swab, randomized  
74 by order of swab type. Combining results from both nostrils, foam and flocked swabs were  
75 concordant for viral detection in 22/30 samples (73.3%). Among the 12 samples positive by  
76 flocked swab, 3 were negative by foam swab. Among 14 samples positive by foam swab, 5  
77 were negative by flocked swab (**Supp Table 2**). Discrepant results occurred exclusively in  
78 samples with low viral load ( $<4 \log_{10}$  viral copies/mL) (**Table 1**).

79

80 ***Performance characteristics of foam versus flocked swabs for measurement of nasal***  
81 ***viral load.*** We first compared the yield of samples collected using foam versus flocked swabs  
82 within the same nostril. All study participants provided paired specimens from both nostrils to  
83 allow for direct comparison. The agreement between samples collected by foam and flocked  
84 swabs was generally high, particularly with high viral load samples, with no evidence of higher  
85 yield with one method versus the other (**Fig 1a**).

86

87 ***Focality of respiratory virus shedding in nasal passages.*** In the same dataset, we  
88 compared swab samples obtained with the same swab type from separate nostrils with a total of  
89 15 paired samples. The values for these viral loads were notably higher in one nostril than the  
90 other and were less in agreement (**Fig 1b**). Moreover, the value from the highest nostril strongly  
91 agreed with the sum of the two nostrils suggesting that a majority of sampled virus comes from  
92 one side (**Fig 1c**) and that sampling the other side underestimates viral load. Therefore, bilateral  
93 sampling is likely required for optimal yield and accurate quantitation.

94  
95 ***Comfort and ease of self-collected foam swabs compared to flocked swabs.*** There was a  
96 trend suggesting that participants found foam swabs more comfortable (9/15 participants agreed  
97 or strongly agreed that the foam swabs were comfortable to use, whereas 4/15 participants  
98 agreed or strongly agreed that flocked swabs were comfortable) although this did not reach  
99 statistical significance ( $p=0.13$ ). Foam swabs were also reported to be easy to collect (14/15  
100 participants agreed or strongly agreed for foam swabs vs 11/15 for flocked swabs;  $p=0.25$ ).  
101 Almost all participants (14/15) would consider participating in future research using foam swabs,  
102 but only 10/15 if flocked swabs are used ( $p=0.13$ ).

103  
104 ***Ease, comfort and high compliance associated with longitudinal nasal sampling during***  
105 ***an upper respiratory virus infection.*** We next enrolled a cohort of 9 otherwise healthy, adult  
106 study participants who self-sampled their nasal passage serially for 14 days, starting within 3  
107 days of upper respiratory symptoms. One participant contributed serial samples twice. Overall  
108 compliance was high: median number of sample days was 14 (range 11-19 days). After  
109 completion of the sample collection period, 70% of participants agreed or strongly agreed that  
110 the foam swab was comfortable, 90% agreed or strongly agreed that the foam swab was easy,  
111 and 80% agreed or strongly agreed that they would participate in future research with foam  
112 swabs. Additionally, 80% of participants agreed or strongly agreed that the swab collection

113 instructions were easy to follow, and 90% agreed or strongly agreed that the collection kit return  
114 process was easy. Serial home-based testing appears to be a well-accepted methodology.

115  
116 ***Steady-state nasal passage viral load kinetics during respiratory virus infections.*** In the  
117 longitudinal sampling portion of our study, we were able to detect 14 viruses including seven  
118 human rhinovirus (HRV), two coronavirus (CoV), one bocavirus (BoV), two adenovirus (ADV),  
119 one human metapneumovirus (MPV) and one respiratory syncytial virus (RSV) cases. There  
120 were four instances of viral co-infection, though in each case a dominant virus was evident  
121 based on greater duration of shedding and higher viral load (**Fig 2a**).

122  
123 Duration of shedding was heterogeneous. In 5 cases, HRV shedding lasted more than a week  
124 with one instance of 5-day shedding and one short single-day blip. RSV and MPV episodes  
125 were both prolonged. ADV, BoV and CoV shedding was short-lived, though in one case low-  
126 level ADV shedding was evident throughout the sampling period (**Fig 2a**).

127  
128 During most extended periods of HRV, RSV and HMPV shedding, viral loads were remarkably  
129 stable from sample to sample (**Fig 2a**). For HRV, a generalized pattern of viral load steady state  
130 or slight gradual decline, followed by rapid elimination was noted. The single case of RSV had a  
131 similar profile but with an initial high viral load peak and shorter duration of shedding. The single  
132 case of MPV had a more protracted decline with a single re-expansion phase. These transiently  
133 observed periods of steady state viral loads are highly unlikely to occur by chance if true viral  
134 loads fluctuated or exhibited stochastic noise. Thus, the sampling method appears highly  
135 reliable. These data also suggest a brief period of equilibrium between the virus and local  
136 immune system before viral elimination.

137

138 ***Viral load kinetics as a predictor of respiratory virus symptoms.*** In general, the level of  
139 symptoms appeared to track with detectable virus, particularly for COV, HRV and MPV. For the  
140 single case of RSV, a high number of symptoms persisted beyond viral elimination (**Fig 2a**). For  
141 all HRV infections of greater than one day, duration of shedding correlated strongly with  
142 duration of symptoms ( $r=0.87$ ). In these HRV infected individuals, symptoms subsided  
143 immediately before, concurrent with or soon after viral elimination. Low viral load infections  
144 lasting only a day were associated with a smaller number of symptoms than more prolonged  
145 higher viral load episodes (**Fig 2a**).

146  
147 ***Stable and surging nasal cytokine levels during respiratory virus infection.*** We next  
148 followed the levels of 20 different cytokines during infection measured from the same specimens  
149 from which the viral load was measured. For several cytokines particularly those in the Th2,  
150 Th17 and non-defined pathways (IL-2, IL-4, IL-5, IL-10, IL-13, IL-17A and eotaxin), there was  
151 notable stability within and between study participants, independent of viral shedding (**Fig 2b**,  
152 **Supp Fig 2b**). Interferon  $\alpha 2a$  also was relatively invariant across and within persons. This result  
153 demonstrates consistency in swabbing technique and yield for molecules that are not impacted  
154 by the presence of viral infection, and again validates the precision of our approach.

155  
156 Other molecules, particularly those associated with cytotoxic T cell responses (granzyme B,  
157 perforin, TNF $\alpha$  and IFN $\gamma$ ) and macrophage responses (MIP-1 $\alpha$ , IL-1 $\alpha$ , IL-6, IL-18) showed  
158 monotonic expansion or clearance in response to most infections, with particularly dynamic  
159 shifts during the examples of RSV, HPMV and one instance of HRV (p21) with the highest initial  
160 viral load (**Fig 2b**, **Supp Fig 2b**). Other cytokines such as IL-12p70, IL-21, IL-5 and IL-18 were  
161 dynamic in participants had monotonic expansion and clearance in response to some but not all  
162 infections.

163



164 **Cytokines correlations according to cellular origin.** We next examined the six participants  
165 with HRV infection for any correlated cytokine patterns to infer cellular origin. Examples of high  
166 positive correlations were noted among analytes associated with a cytotoxic T cell response  
167 (granzyme B, perforin, TNF $\alpha$ , and IL-6), among several macrophage or epithelial cell derived  
168 cytokines (MIP-1 $\alpha$ , IL1 $\alpha$ , IL-6, IL-12p70, IL-21), and among a cluster associated with Th2  
169 responses (IL-5, IL-10, IL-17). The Th2 associated cytokines (IL-5, IL-10, IL-17) also correlated  
170 with many of the cytolytic T cell and macrophage associated cytokines (**Fig 3a**). HRV viral load  
171 was only moderately correlated with a number of parameters, particularly granzyme B, perforin,  
172 and IP10 which is a protein induced by IFN $\gamma$ . This result suggests that HRV may not induce an  
173 intense local molecular immune response in a dose-dependent fashion. Very similar results  
174 occurred with inclusion of all samples from all participants in the cohort (**Supp Fig 3a**).

175  
176 We next examined cytokine correlations in the 2 persons infected with more inflammatory  
177 respiratory viruses: RSV and MPV. We noted similar correlative trends in this data as with HRV.  
178 Correlations among related pairs such as granzyme B / perforin, IL-12p70 / IL-21, IL-1 / MIP-  
179 1alpha, IL-5 / IL-18, TNF-alpha / IL-6, IL-10 / IL-17a and IL-2 / IL-4 were higher for RSV / MPV  
180 than for HRV (**Fig 3b**). For these cytokine pairs, temporal kinetics were often strikingly similar  
181 suggesting an equivalent cellular source (**Fig 2b, Supp Fig 2b**). There was also an overall lack  
182 of correlation between cytokines associated T cells responses and those associated with  
183 epithelial cells and macrophages. Viral load correlated with many cytokines of T cell origin (**Fig**  
184 **3b**), suggesting that RSV and MPV may induce inflammation in a dose-dependent fashion.

185  
186 **Sample clustering according to degree of inflammation.** We next sorted all HRV samples  
187 using linkage clustering analysis. This approach demonstrated three classes of samples that  
188 were distinguished by the levels of many of the T-cell and macrophage-associated molecular  
189 immune factors (**Fig 3b**). The minority of samples (blue class) with the highest levels of

190 granzyme B, perforin, IL-6, IL-1 $\alpha$ , MIP-1 $\alpha$  and IFN $\gamma$  all had high viral loads. These samples were  
191 from two participants. All six participants had some samples in the least inflammatory class  
192 (grey) and 5 participants had samples in the moderate inflammatory class (green). These data  
193 indicate that the inflammatory immune milieu in the HRV-infected nasal passage is dynamic  
194 over time, but tilts toward higher inflammation with higher viral loads. Very similar results were  
195 observed when all samples were analyzed though only two classes of samples were  
196 distinguished (**Supp Fig 3b**).

197

198 We next sorted the RSV and MPV samples using linkage clustering and could not identify the  
199 optimal number of clusters. We selected two clusters which were differentiated according to  
200 concentrations of most cytokines, again including granzyme B, perforin, IL-6, IL-1 $\alpha$ , MIP-1 $\alpha$  and  
201 IFN $\gamma$ . In the case of these viruses, the more inflammatory cytokine cluster clearly associated  
202 with high viral loads for both RSV and MPV (**Fig 3d**).

203

204 ***Mathematical modeling.*** We performed mathematical modeling separately on data from the  
205 participant infected with RSV to examine whether complex immune and viral data from our  
206 samples could be coupled mechanistically. We first developed the ordinary differential equation  
207 model in equation (1) to link RSV viral load and early and late immune responses and evaluated  
208 which cytokines may track those responses. For the early immune response, we found that only  
209 the log<sub>10</sub> of the concentration change of IFN- $\gamma$  and IP-10 was positively correlated to the viral  
210 load during the first 5 days after enrollment (**Supp Fig 4a-b**), so we evaluated models for only  
211 these two cytokines to track the RSV-early immune response. For the late immune responses,  
212 we evaluated the model for fit to all observed cytokines (**Supp Fig 4c**). An equivalent approach  
213 was carried forward to model MPV.

214

215 In **Fig 4a**, we show our resulting model schematic. Differential equations capture the rate of  
216 change of susceptible cells, infected cells, viral load (**Fig 4b**) and two cytokines (**Fig 4c-d**). The  
217 best fit was achieved with a model assuming IFN $\gamma$  concentration dependent killing during the  
218 first early stages of infection, and IL-21 mediated elimination of infected cells with a mechanism  
219 saturating the amount of possible killing above a certain level of IL-21.

220

221 The model suggests that for RSV, an early surge in IFN $\gamma$  leads to a slight rise in per cell killing  
222 rate of infected cells (**Fig 4e**) leading to a mass elimination of infected cells at a rate of 10  
223 million cells per day and a decrease in viral load by a factor of 100-1000. However, this  
224 response does not clear the virus. A steady state viral load persists for 4 days until an IL-21  
225 mediated response appears. This response kills far more rapidly, but not as intensely as the  
226 IFN $\gamma$  response. Together, these responses remove the remaining infected cells by day 7 after  
227 onset of symptoms (**Fig 4f**). Model fitting using data in which IP10 provides early clearance  
228 rather than IFN $\gamma$  results in worse fit to the data (**Supp Fig 4c, 4d**). For late results, IL-21  
229 allowed the best fit and other cytokines was less successful. This suggests that these two  
230 molecules may play a major role in RSV control in vivo but does not rule out the effects of other  
231 cytokines and effector molecules in limiting infection.

232

233 We next fit the same model to the data from participant infected with MPV and found that the  
234 model is able to recapitulate viral load, IFN $\gamma$  and IL-21, projects similar killing patterns during the  
235 early and late immune responses to the RSV model (**Supp Fig 5**).

236

## 237 **Discussion**

238

239 Here we demonstrate that home self-sampling with nasal foam swabs is well-tolerated and  
240 provides reliable results for monitoring viral load as well as the molecular immune response to

241 respiratory virus infection. These results have enormous practical implications. Self-collection at  
242 home is safe, non-invasive and easily learned, allowing a reliable method for diagnosis as well  
243 as therapeutic monitoring. Because our kits could easily be used at home or in a drive through  
244 testing environment, they provide an avenue to eliminate contact between an infected and  
245 contagious person, and health care providers. They could also be used in the hospital or clinic  
246 setting, thereby saving personnel time and personal protective equipment. The use of  
247 comfortable, safe and affordable foam swabs also highlights the possibility of scaling this  
248 approach to pediatric, adult, elderly and immunocompromised populations. For the current  
249 SARS-CoV-2 pandemic, and future deadly respiratory virus epidemics, home self-swabbing will  
250 be a vital tool.

251  
252 The simplicity of the sampling approach also facilitates large scale research studies of viral  
253 pathogenesis and transmission dynamics in which participants self-sample for months. Our  
254 inability to stop the spread of the COVID-19 epidemic in the United States has demonstrated a  
255 poor overall understanding of cryptic transmission patterns of respiratory viruses. Because our  
256 approach is safe, well accepted, and easy to implement, longitudinal sampling studies within  
257 families, workplaces and at large conferences are highly feasible.

258  
259 We have previously demonstrated increased sensitivity of self-collected foam nasal swabs  
260 compared to nasal washes in immunocompetent adults with respiratory viral infections<sup>24</sup>.  
261 Additional anatomical sites have also been considered for increasing yield, and current FDA  
262 recommendations suggest use of both a mid-turbinate nasal swab and an oropharyngeal swab  
263 to maximize yield in the absence of nasopharyngeal swabbing<sup>23</sup>. Our prior data demonstrate  
264 that self-collected throat swabs in addition to self-collected foam nasal swabs do not increase  
265 yield significantly for respiratory viruses<sup>26</sup>, suggesting that additional oral swabbing may not be  
266 needed, especially in the setting of swab shortages. Self-collected foam swabs have been used

267 for longitudinal studies in solid organ transplant recipients<sup>25</sup>, with good compliance and  
268 participants reporting no issues with swab discomfort. The specific swab used in these prior  
269 studies and our present study were custom designed to limit discomfort while maintaining  
270 adequate sensitivity; we have demonstrated stability with these swabs with and without  
271 transport media after storage at room temperature for 7 days<sup>24</sup>, making them ideal for home  
272 self-testing followed by shipment directly to a testing lab. Furthermore, SARS-CoV-2 has been  
273 shown to be highly stable on surfaces<sup>27</sup>, making home foam swabbing a feasible and attractive  
274 option for this pathogen.

275  
276 We also demonstrate an ability to accurately sample local cytokines which are present at  
277 picogram levels, again using the same foam swabs from which viral measurements were made.  
278 The combination of precise virologic and immunologic readouts of local infection is highly  
279 relevant for developing clinical severity scores and biomarkers. While studies are beginning to  
280 show that viral load may be predictive of COVID-19 severity<sup>10</sup>, it is equally plausible that the  
281 intensity and phenotype of the early local cellular immune response plays a causal role in  
282 limiting the extent of infection<sup>28</sup>. By following the molecular immune response closely with daily  
283 sampling intervals, we also provide adequate data for mathematical models that can link  
284 specific arms of the cellular immune response to pathogen control in real time<sup>22</sup>, a goal that has  
285 been difficult to attain for a majority of viral infections in humans.

286  
287 Our study demonstrates several novel features of respiratory virus kinetics. RSV infection  
288 achieves a brief, extremely high, viral load, followed by a steady state and a final rapid phase of  
289 elimination. HRV also has a remarkably stable viral load in most participants before being  
290 rapidly eliminated. During a majority of our observed episodes, viral shedding is strongly  
291 correlated with symptoms. As viral load decreases, symptoms tend to dissipate.

292

293 Certain molecular immune responses are constitutively expressed, and vary little between and  
294 within participants, particularly those associated with Th2 mechanisms that are unlikely to play a  
295 role in elimination of virally infected cells. On the other hand, small molecules associated  
296 specifically with tissue-resident T cell responses such as granzyme B, perforin and IFN $\gamma$ , and  
297 macrophages such as IL-6 and IL-1 expand and contract during the course of viral shedding,  
298 particularly with more severe infections such as RSV and HPMV. Our technique therefore  
299 overcomes a fundamental limitation of human immunological studies, which is the inability to  
300 sample over temporally granular time intervals at the mucosal site of viral replication.

301  
302 Further validation of our technique is demonstrated with mathematical modeling that links  
303 expression of certain cytokines with early and late elimination of virus. For RSV and MPV, we  
304 demonstrate that an early surge in IFN $\gamma$  is coupled with elimination of a massive number of  
305 infected cells but is insufficient for complete containment of infection, which is achieved several  
306 days later concurrent with slower expansion IL-21. Notably, IL-21 has previously been identified  
307 as required for RSV elimination in murine models<sup>29-31</sup> In our model, it induces an extremely high  
308 death rate of infected cells once above a certain concentration. Larger scale studies may be  
309 able to link surges in different cytokines with different respiratory viruses, including SARS CoV-  
310 2, and to differentiate severity using these techniques. Of particular interest is combining  
311 information on levels of *local* cytokine levels with viral load at presentation, along with patient  
312 metadata, to predict infection severity.

313  
314 There are important limitations to our study. Correlations between foam and flocked swabs were  
315 weaker at low viral loads. However, stochastic variation in low viral load samples is inherent to  
316 quantitation of viruses which replicate in mucosa. Additional variables such as storage  
317 temperature may have contributed to viral quantification variability. Our samples size for  
318 longitudinal episodes is relatively low, particularly when considered on a per virus basis. A

319 greater number of participants will be required to definitively differentiate kinetics patterns of  
320 different respiratory viruses, as well as the cytokine profiles associated with their containment.  
321 Selection of cytokines as incomplete and may have missed critical responders to viral infection.  
322 Our mathematical models dramatically oversimplify the coordinated immune response against  
323 the virus but do generate testable hypotheses that IFN $\gamma$  and IL-21 are viral for early and late  
324 containment of infection.

325  
326 In summary, we establish a foam swab-based sampling method that is optimal for patient self-  
327 testing, both at home and in the clinical setting, permits serial therapeutic monitoring, and is  
328 suitable for tracking the natural virologic and immunologic course of respiratory virus infections.  
329 We recommend that this method be adapted to future clinical and research applications,  
330 including for the study of SARS-CoV-2.

331

332 **Methods.**

333

334 ***Protocol.***

335 The study was approved by the Institutional Review Board at Fred Hutchinson Cancer Research  
336 Center.

337

338 *Flocked vs foam swab study:* Participants with symptoms of an acute respiratory illness, defined  
339 as the presence of respiratory symptoms (**Supp Table 1**) for less than 3 days, were enrolled in  
340 the study. Each participant completed 2 sample collections, each separated by one hour. At  
341 each time point, the participant collected either a) two self-collected Copan flocked swabs (#23-  
342 600-966), one from each nostril or b) two self-collected Puritan foam swabs (Puritan Medical  
343 Red #25-1805-SC 2), one from each nostril. The foam swab was designed in a mushroom  
344 shape to maximize swabbing from the nostril wall (**Supp Fig 1**) and has been used in previous  
345 studies in HCT and lung transplant recipients<sup>24,25</sup>. Foam and flocked swabs were self-collected  
346 following instruction by trained study personnel. Participants used a saline spray bottle with a  
347 nozzle to dispense 5 sprays into one nostril. The participant then placed the swab into the  
348 moistened nostril and rotated the swabs and blew for about 5 seconds or 5 rotations. Following  
349 sample collection, participants were asked to complete a brief survey to assess the tolerability  
350 and acceptability of the various testing methods.

351

352 Immediately following collection, each nasal swab was placed in a conical vial containing 1000ul  
353 of cytokine preservative buffer consisting of phosphate buffered saline (PBS) with 10% Igepal,  
354 1% protease inhibitor cocktail (EMD Millipore: 539131-1VL), and 0.25% bovine serum albumin  
355 (BSA; Sigma A7906-100G). All swabs from the right nostril were stored at -20°C; all swabs from  
356 the left nostril were stored at 4°C. All samples were stored for 1 week prior to processing. Swab  
357 collection order (flocked vs foam) was randomized using an online randomization tool



358 (www.randomizer.org). To compare the number of participants who agreed or strongly agreed  
359 with statements regarding comfort, ease of use, and participation in future research for foam  
360 versus flocked swabs, we used McNemar's test with exact p-values.

361  
362 *Longitudinal sampling study:* Participants with symptoms of an acute respiratory illness, defined  
363 as presence of respiratory symptoms (**Supp Table 1**) for less than 3 days, were enrolled in the  
364 study. Each participant collected two Puritan foam nasal swabs, one from each nostril, per day  
365 for 14 days after enrollment or until symptoms resolved, whichever was longer. Participants  
366 completed a daily electronic symptom survey, in which participants were asked to record the  
367 presence and severity of symptoms in specific categories: nasal, eyes, ears, throat, chest,  
368 gastrointestinal, general, sleep and sensory changes (**Supp Table 1**). Following completion of  
369 the 14-day sample collection, participants were asked to complete a brief survey to assess the  
370 tolerability and acceptability of the testing methods.

371  
372 Immediately following collection, each nasal swab was placed in a conical vial containing 1000ul  
373 of cytokine preservative buffer consisting of 0.1% Tween 20, 1% protease inhibitor (EMD  
374 Millipore: 539131-1VL), 1% BSA (Sigma A7906-100G), 1X ProClin300 (at 1:2000, diluted with  
375 PBS). Participants were instructed to store collected swabs in the participant's home  
376 refrigerator. Participants then transported collected samples to the lab in insulated bags  
377 containing ice packs within one week of sample collection. Nasal swabs were processed within  
378 one week of sample collection. Collections from each nostril were combined for the final  
379 analyses.

380  
381 ***Lab methods.***

382 *Sample processing:* Each conical vial containing a swab was vortexed and 500ul of buffer was  
383 removed and stored at -80°C for PCR analysis. The swab was then removed from the conical

384 vial and placed in a pre-chilled 0.45um SPIN-X filter and the handle of the swab was removed.  
385 The buffer remaining in the conical vial was then transferred to the SPIN-X filter containing the  
386 swab. The SPIN-X filter was then spun at 13000xg for 15 minutes at 4°C with no brake. 300ul of  
387 fresh cytokine preservative buffer was then added to the SPIN-X filter which was then incubated  
388 on wet ice for 5 minutes then spun again at 13000xg for 30 minutes at 4°C with no brake. The  
389 swab and filter were discarded, and the filtered buffer was then aliquoted in 100ul increments  
390 and stored at -80°C until further testing.

391

392 *Viral testing:* Nasal swab specimens were tested using a multiplex PCR testing for 11  
393 respiratory viruses [adenovirus A-F, human rhinovirus (HRV), influenza A and B, parainfluenza  
394 viruses (PIV) 1-4, human coronavirus (CoV), bocavirus (BoV), respiratory syncytial virus (RSV)  
395 and human metapneumovirus (MPV)] as previously described<sup>32</sup>.

396

397 *Cytokine testing:* Cytokine levels were quantified in nasal specimens using the  
398 electrochemiluminescence-based Mesoscale Discovery (MSD) platform. For the longitudinal  
399 sampling study, the following panels were used: U-PLEX Biomarker Group 1 (Eotaxin, IFN- $\alpha$ 2a,  
400 IL-1, IL-8, IL-12p70, IL-13, IL-18, IL-21, IP-10, MIP-1 $\alpha$ ), U-PLEX Custom Biomarker (IFN- $\gamma$ , IL-2,  
401 IL-4, IL-5, IL-6, IL-10, IL-17A, TNF- $\alpha$ ), R-PLEX Granzyme B, and R-PLEX Perforin. Preparation  
402 of analyte detection plates was done following the manufacturer's instructions (Meso Scale  
403 Diagnostics). A series of 8 concentrations of biomarkers standards and the test samples were  
404 added in duplicates to the wells. The plates were incubated shaking for 1 hour. In parallel to  
405 plate incubation, the plate-respective SULFO-TAG labeled detection antibodies were combined.  
406 The plates were washed, and the respective detection antibody mixture was added to each well.  
407 The plates were incubated shaking for 1 hour. Plates were washed, then 2X Read buffer was  
408 added to each well. The plates were read on the MSD Plate reader (MESO QuickPlex SQ 120).  
409 Protein concentrations were determined using the MSD Discovery Workbench 4.0 analysis

410 software. The light intensities from samples were interpolated using a four-parameter logistic fit  
411 to a standard curve of electrochemiluminescence generated from the known concentrations of  
412 the standards. The lower limit of detection for each marker can be found on the manufacturer's  
413 website: <https://www.mesoscale.com/~media/files/handouts/assaylist.pdf>.

414  
415 **Statistical analysis.** For the foam versus flocked swab study, PCR results that were positive on  
416 the qualitative assay but below the limit of detection were imputed as 500 copies per ml, using  
417 the limit of detection divided by two. PCR results were log<sub>10</sub>-transformed and negative results  
418 were assigned a value of 0. The concordance correlation coefficient (CCC) was used to  
419 measure agreement of quantitative results between paired samples (foam versus flocked  
420 swabs, left versus right nostril samples, sum versus maximum value from left and right  
421 nostrils)<sup>33</sup>. For the longitudinal sampling study, cytokine results that were below the fitted curve  
422 range were assigned the value of the lower limit of detection divided by two and results that  
423 were above the fitted curve range were assigned the value of the upper limit of detection.  
424 Results were log<sub>10</sub>-transformed for analysis. Symptoms are represented as the total number of  
425 symptoms present for each day, out of a total of 26 (**Supp Table 1**). SAS, version 9.4 (SAS  
426 Institute, Cary, North Carolina) and Stata, version 16.1 (StataCorp, College Station, Texas)  
427 were used for analysis.

428  
429 **Cytokine clustering.** To check whether the samples could be classified into groups with similar  
430 cytokine concentrations, we performed a cluster analysis of the samples where each sample is  
431 an array of the 20 measured cytokine concentrations. First, we checked for cluster tendency of  
432 the samples using Hopkin statistic (H)<sup>34,35</sup>. H can have values between 0 and 1, where values  
433 close to 1 indicate that the samples are highly clustered and values close to 0.5 indicate random  
434 samples. When calculated H (get\_clust\_tendency function in R3) was greater than 0.5, we did a  
435 linkage hierarchical clustering with Euclidean distances of the samples<sup>36</sup>.

436

437 **Mathematical modeling.**

438 *Model assumptions:* To understand how the immune system drives respiratory virus dynamics  
 439 we used an acute viral infection model that distinguishes between early and late responses to  
 440 RSV. In this model, susceptible cells ( $S$ ) are infected at rate  $\beta VS$  by free RSV virus ( $V$ ). The  
 441 impact of host immunity is tracked by modeling two cytokines that are plausible surrogates for  
 442 those responses. We assumed RSV-infected cells ( $I$ ) are cleared by: (1) an innate response  
 443 with rate  $\kappa_G G$  mediated by an innate immune response tracked by an initial cytokine ( $G$ ); and (2)  
 444 an acquired response with rate  $\frac{\kappa_C C^r}{C^r + \phi^r}$  mediated by an acquired immune response tracked by a  
 445 second cytokine ( $C$ ). The Hill coefficient  $r$  parameterizes the nonlinearity of the response and  
 446 allows for rapid saturation of the killing. In the model,  $G$  is secreted proportionally to the number  
 447 of infected cells with rate  $\omega_G I$  and cleared with rate  $\delta_G G$ .  $C$  is secreted in a non-linear fashion  
 448 with density dependent rate  $\omega_C \frac{I}{I+I_{50}}$  and cleared with rate  $\delta_C C$ . Finally, free virus is produced  
 449 at a rate  $\pi$  and cleared with rate  $\gamma$ . The model is expressed as a schematic (**Fig 4a**) and here as  
 450 a system of ordinary differential equations:

$$\begin{aligned}
 \frac{dS}{dt} &= -\beta VS \\
 \frac{dI}{dt} &= \beta VS - \kappa_G GI - \kappa_C \frac{C^r}{C^r + \phi^r} I \\
 \frac{dV}{dt} &= \pi I - \gamma V \\
 \frac{dG}{dt} &= \omega_G I - \delta_G G \\
 \frac{dC}{dt} &= \omega_C \frac{I}{I+I_{50}} C - \delta_C C
 \end{aligned}
 \tag{1}$$

452 *Selection of surrogate cytokines:* To select the initial cytokine to model the surrogate for early  
 453 immune response ( $G$ ) we performed Pearson's correlation tests between the RSV viral load  
 454 from day 1 until day 5 post-enrollment and the  $\log_{10}$  of the concentration change of each  
 455 cytokine until day 5 post-enrollment. We modeled equation (1) only for the cytokines with  
 456 positive correlation that were statistically significant. Then for each cytokine obtained for

457 variable  $G$  we tried model fitting to all cytokines for variable  $C$  individually. We selected the  
458 surrogate for the acquire immune response to RSV ( $C$ ) the cytokine that gave a lower sum of  
459 squares error in the model fitting.

460

461 *Model fitting: Model fitting:* We performed fitting of model in equation (1) to the data assuming  
462  $t = 0$  as the time of enrollment. We also assumed initial concentrations of  $S(0) = 10^7$  cells/ $\mu\text{L}$ ,  
463  $I(0) = \frac{\pi V(0)}{\gamma}$  and obtained  $V(0)$ ,  $G(0)$  and  $C(0)$  from the viral load and cytokine initial  
464 concentrations, respectively. We estimated the remaining best parameters using nonlinear  
465 least-squares. Implementation used the differential evolution (DEoptim) and the L-BFGS-B  
466 (optim) algorithms in R.

467

468 *Model predictions:* We used equation (1) and best estimates from the best model fits to  
469 calculate the absolute number of infected cells killed and the killing rate per cell during early and  
470 late immune responses against RSV. The number of eliminated infected cells at any time was  
471 calculated by the equations  $\kappa_G GI$  and  $\kappa_C \frac{C^r}{C^r + \phi^r} I$  for the early and late responses, respectively.

472 Similarly, we computed the killing rate per cell during early and late response as  $\kappa_G G$  and

473  $\kappa_C \frac{C^r}{C^r + \phi^r}$ .

474 **Acknowledgements**

475 We would like to thank our study participants.

476

477 **Author Contributions**

478 AW designed the experiments and wrote the manuscript. EMK performed statistical analysis,  
479 SB performed statistical analysis and mathematical modeling. EV performed data analysis. TL  
480 enrolled participants and performed experiments. ELC enrolled participants and performed  
481 experiments. UP performed the cytokine analysis. JK performed respiratory virus PCR. ERD  
482 wrote the manuscript. KRJ designed the respiratory virus PCR. ALG performed the respiratory  
483 virus PCR. DBR performed mathematical modeling. EFCO performed mathematical modeling.  
484 MB designed the experiments and wrote the manuscript. JTS designed the experiments,  
485 designed the mathematical modeling and wrote the manuscript.

486

487 **Funding Statement**

488 This work was supported by the National Institutes of Health [grant numbers K24 HL093294-06  
489 (M.B.), K23 AI114844-02 (A.W.)] and the Fred Hutchinson Cancer Center Vaccine and  
490 Infectious Diseases Faculty Initiative Fund (M.B. and J.S.).

491

492 **Competing Interests Statement**

493 A.W.: Kyorin (personal fees), Ansun (research support), VB Tech (research support), all outside  
494 of the submitted work. A.G.: Abbott Molecular, personal fees, outside of the submitted work.  
495 M.B.: Kyorin (personal fees), Gilead (research support, personal fees), ReViral (personal fees),  
496 Janssen (research support, personal fees), Ansun (research support, personal fees), Moderna  
497 (personal fees); Vir Bio (research support, personal fees); GSK (personal fees), Pulmocide  
498 (personal fees), VB Tech (research support), Bavarian Nordic (personal fees), DMA (personal  
499 fees), Allovir (personal fees), all outside of the submitted work.

500 **Figure legends**

501

502 **Figure 1: Comparison of viral loads between self-collected foam and flocked swabs. (a)**

503 Viral loads from the same nostril using flocked and foam swabs are concordant, particularly at  
504 higher viral loads. **(b)** Differential viral loads with the same swab type, observed between  
505 nostrils, show moderate concordance. **(c)** Viral load from the highest nostril strongly agrees with  
506 the sum of the two nostrils suggesting that a majority of sampled virus comes from one side.  
507 Overlapping data points have been jittered to allow viewing of all data points. CCC =  
508 concordance correlation coefficient; CoV = coronavirus; FluA = Influenza A; HRV = human  
509 rhinovirus; PIV3 = parainfluenza virus 3; RSV = respiratory syncytial virus.

510

511 **Figure 2: Viral load, symptoms and cytokine levels in serial sampling in both nostrils.**

512 Each row represents a participant. **(a)** Viral load (lines) and quantity of symptoms (bars) are  
513 shown on left and often tracked with each other longitudinally. Serial sampling in both nostrils  
514 with foam swabs reveals a steady state for HRV, RSV and HMPV viral loads prior to rapid  
515 elimination. **(b)** Levels for each cytokine (granzyme B, perforin, IFN $\gamma$ , IP-10, MIP-1 $\alpha$ , IL-1 $\alpha$ , IL-6,  
516 TNF-  $\alpha$ , IL-20p70, IL-21) are shown on the right. Paired cytokines show concordant expansion  
517 and clearance phases. HRV = human rhinovirus; RSV = respiratory syncytial virus; MPV =  
518 metapneumovirus; ADV = adenovirus; CoV = coronavirus, BoV = bocavirus.

519

520 **Figure 3: Cytokines correlate according to cellular origin during respiratory virus**

521 **infection, while samples cluster according to level of inflammation. (a, b)** Data from  
522 participants p16, p17, p18, p19, p20, p21 and p22b who have HRV infection. **(c, d)** Data from  
523 participants p22 and p23 who have RSV and MPV respectively. **(a, c)** Correlation plots with  
524 strong correlation according to cell type origin. X indicates a non-significant correlation. Color  
525 intensity and the size of the dot are proportional to the Pearson correlation coefficient. For both

526 datasets, strong positive correlations are noted within cytokines linked with cytolytic T-cell  
527 responses; macrophage responses; and T<sub>H</sub>2 responses. **(b, d)** Linkage clustering analysis of  
528 samples (columns) demonstrates classes of samples based on the concentration of  
529 inflammatory cytokines. **(b)** For HRV infections, a minority of samples (blue class) from 2  
530 participants and with the highest levels granzyme B, perforin, IL-6, IL-1 $\alpha$ , MIP-1 $\alpha$  and IFN $\gamma$  all  
531 had high viral loads. All six participants had samples in the least inflammatory class (grey) and  
532 five participants had samples in the moderate inflammatory class (green). **(d)** For RSV and  
533 MPV, inflammatory (blue) and non-inflammatory (green) sample clusters are evident. The  
534 inflammatory class of samples is highly associated with the highest viral loads. VL = viral load;  
535 DL = detection limit.

536

537 **Figure 4: Mathematical modeling of a single participant's RSV kinetics and the early and**  
538 **late immune responses tracked by IFN- $\gamma$  and IL-21.** **(a)** Schematic representation of the  
539 model. S represents cells susceptible to RSV; I, RSV-infected cells; V, RSV virions; G, IFN- $\gamma$   
540 concentration and C, IL-21 concentration. Best fit models to **(b)** viral load, **(c)** IFN- $\gamma$  and **(d)** IL-  
541 21 measurements using a nonlinear least-squares approach. Circles represent the data, and  
542 black-solid lines the best model predictions. Models fit better to these cytokines than all others  
543 charted in **Fig 2** and **Sup fig 2**. **(e)** Model estimates of the killing rate per cell of infected cells  
544 mediated by IFN- $\gamma$  and IL-21, calculated as  $\kappa_G G$  and  $\kappa_C \frac{C^r}{C^r + \phi^r}$ , respectively. **(f)** Total number of  
545 infected cell deaths mediated by IFN- $\gamma$  and IL-21, computed as  $\kappa_G G I$  and  $\kappa_C \frac{C^r}{C^r + \phi^r} I$ ,  
546 respectively. In **(e)** and **(f)** blue and green lines represent model predictions of the effects  
547 mediated by IFN- $\gamma$  and IL-21, respectively.

548

549 **Supplemental Figure 1: Image of Puritan foam swab (Puritan Medical Red #25-1805-SC 2)**  
550 **used in swab comparison and longitudinal sampling study.**



551

552 **Supplemental Figure 2: Symptoms, viral load and cytokine levels in serial sampling in**  
553 **both nostrils in all participants for remainder of cytokines evaluated.** Each row represents  
554 a participant. **(a)** Viral load (lines) and quantity of symptoms (bars) are shown on left and often  
555 tracked with each other longitudinally. Serial sampling in both nostrils with foam swabs reveals a  
556 steady state for HRV, RSV and HMPV viral loads prior to rapid elimination. **(b)** Levels for each  
557 cytokine are shown on the right. Paired cytokines show concordant kinetics. HRV = human  
558 rhinovirus; RSV = respiratory syncytial virus; MPV = metapneumovirus; ADV = adenovirus; CoV  
559 = coronavirus, BoV = bocavirus.

560

561 **Supplemental Figure 3: Cytokines correlate according to cellular origin during**  
562 **respiratory virus infection, while samples cluster according to level of inflammation.** Data  
563 is from all participants. **(a)** Correlation plot with strong correlation according to cell type origin. X  
564 indicates a non-significant correlation. Color intensity and the size of the dot are proportional to  
565 the Pearson correlation coefficient. Strong positive correlations are noted within cytokines linked  
566 with cytolytic T cell responses; macrophage responses; and T<sub>H2</sub> responses. **(b)** Linkage  
567 clustering analysis of all samples demonstrates classes of samples based on the concentration  
568 of inflammatory cytokines. A minority of samples (grey class) had highest levels granzyme B,  
569 perforin, IL-6, IL-1 $\alpha$ , MIP-1 $\alpha$  and IFN $\gamma$ . VL = viral load; DL = detection limit.

570

571 **Supplemental Figure 4: Selection of surrogate cytokines for modeling early and late**  
572 **immune responses against RSV.** Scatterplot between RSV viral load from days 1 to 5 post  
573 enrollment and the log<sub>10</sub> concentration of **(a)** IFN $\gamma$  and **(b)** IP-10 until day 5 post enrollment. p-  
574 values and correlation coefficient obtained using Pearson's test. Correlation test for all other  
575 cytokines was not statistically significant. **(c)** Sum of squared error (SSE) of the best model fits  
576 of equation (1) assuming early response (G) is tracked by IFN $\gamma$  and late response (C) is tracked

577 by each of the cytokines in x-axis. Lowest SSE (best fit) is obtained when late response is  
578 tracked by IL-21. **(d)** Sum of squared error (SSE) of the best model fits of equation (1)  
579 assuming early response ( $G$ ) is tracked by IP10 and late response ( $C$ ) is tracked by each of the  
580 cytokines in x-axis. Lowest SSE (best fit) is obtained when late response is tracked by IL-21.

581

582 **Supplemental Figure 5. Mathematical modeling of a single participant's MPV kinetics and**

583 **the early and late immune responses tracked by IFN- $\gamma$  and IL-21. (a)** Schematic

584 representation of the model.  $S$  represents cells susceptible to MPV;  $I$ , MPV-infected cells;  $V$ ,

585 RSV virions;  $G$ , IFN- $\gamma$  concentration and  $C$ , IL-21 concentration. Best fit models to **(b)** viral load,

586 **(c)** IFN- $\gamma$  and **(d)** IL-21 measurements using a nonlinear least-squares approach. Circles

587 represent the data, and black-solid lines the best model predictions. Models fit better to these

588 cytokines than all others charted in **Fig 2** and **Sup fig 2**. **(e)** Model estimates of the killing rate

589 per cell of infected cells mediated by IFN- $\gamma$  and IL-21, calculated as  $\kappa_G G$  and  $\kappa_C \frac{C^r}{C^r + \phi^r}$ ,

590 respectively. **(f)** Total number of infected cell deaths mediated by IFN- $\gamma$  and IL-21, computed as

591  $\kappa_G G I$  and  $\kappa_C \frac{C^r}{C^r + \phi^r} I$ , respectively. In **(e)** and **(f)** blue and green lines represent model predictions

592 of the effects mediated by IFN- $\gamma$  and IL-21, respectively.

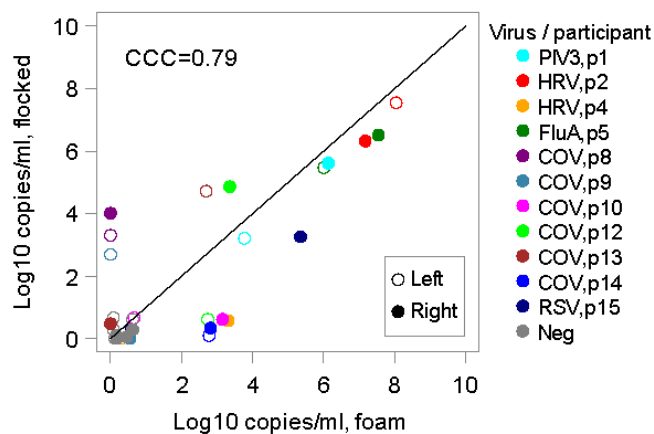
**Table 1: Viral loads in matched foam versus flocked swabs in participants with new onset respiratory symptoms.**

Participant number	Virus	Foam right Log10 copies/ml	Foam left Log10 copies/ml	Flocked right Log10 copies/ml	Flocked left Log10 copies/ml
p1	PIV3	6.12	3.79	5.64	3.19
p2	HRV	7.18	8.02	6.35	7.54
p3	neg	0	0	0	0
p4	HRV	2.70	0	0	0
p5	FluA	7.53	6.00	6.52	5.48
p6	neg	0	0	0	0
p7	neg	0	0	0	0
p8	COV	0	0	3.99	3.29
p9	COV	0	0	0	2.70
p10	COV	2.70	0	0	0
p11	neg	0	0	0	0
p12	COV	3.40	2.70	4.84	0
p13	COV	0	2.70	0	4.71
p14	COV	2.70	2.70	0	0
p15	RSV	5.34	0	3.26	0

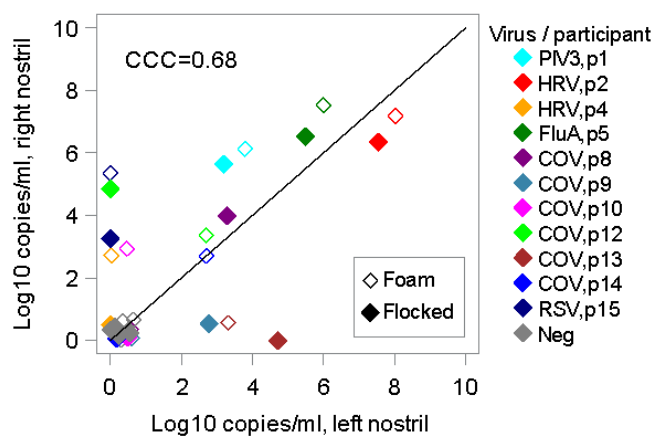
PIV = parainfluenza virus; HRV = human rhinovirus; FluA = influenza virus A; COV = coronavirus; RSV = respiratory syncytial virus

**Figure 1**

a) Flocked vs. foam swabs



b) Right vs. left nostril



c) Sum vs. max of left and right nostrils

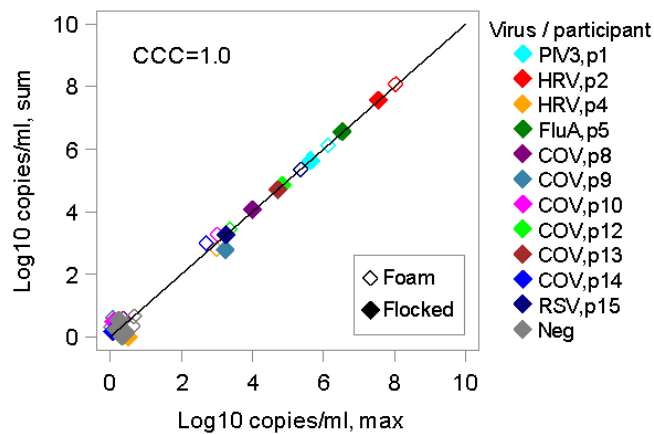


Figure 2

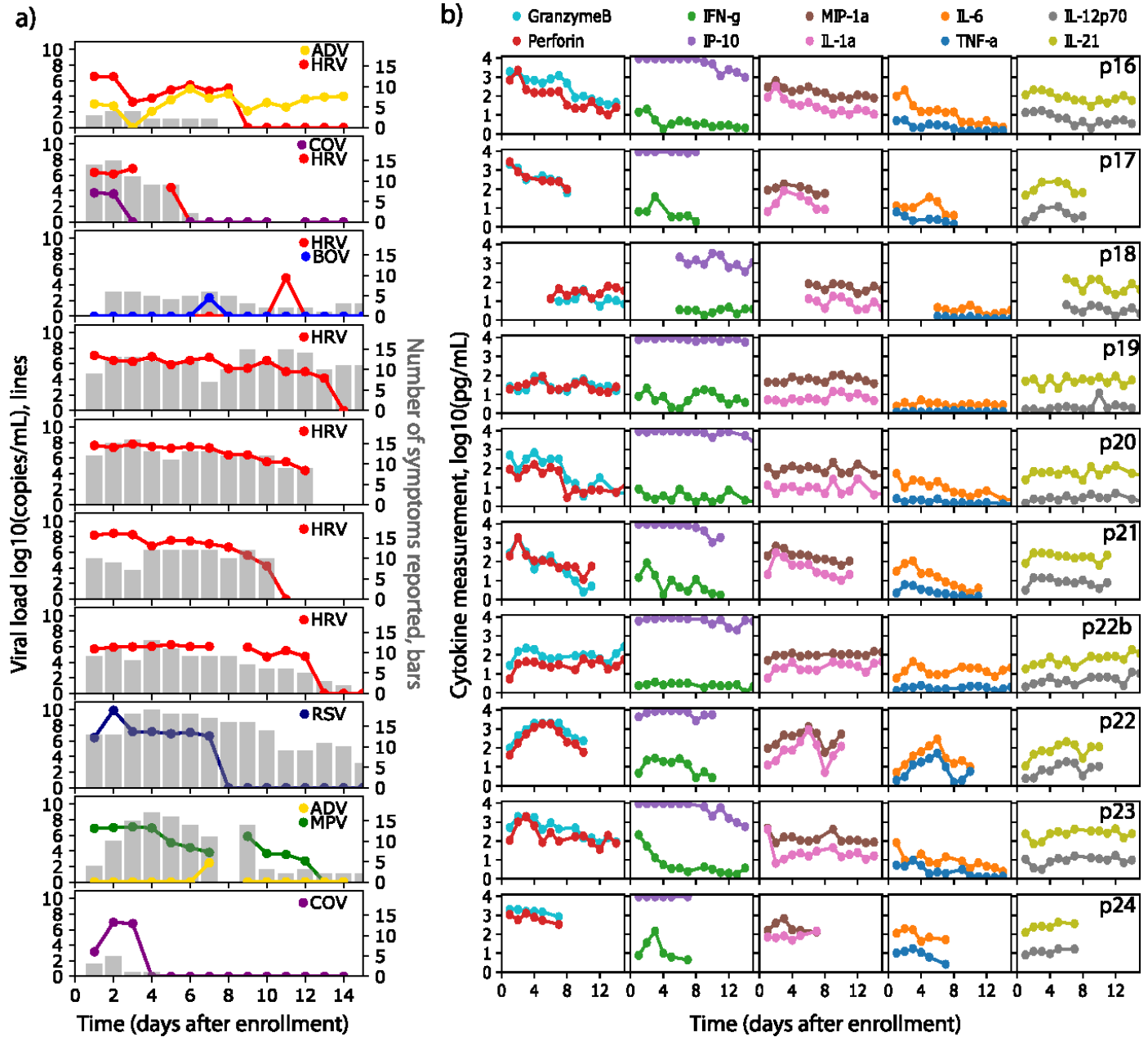
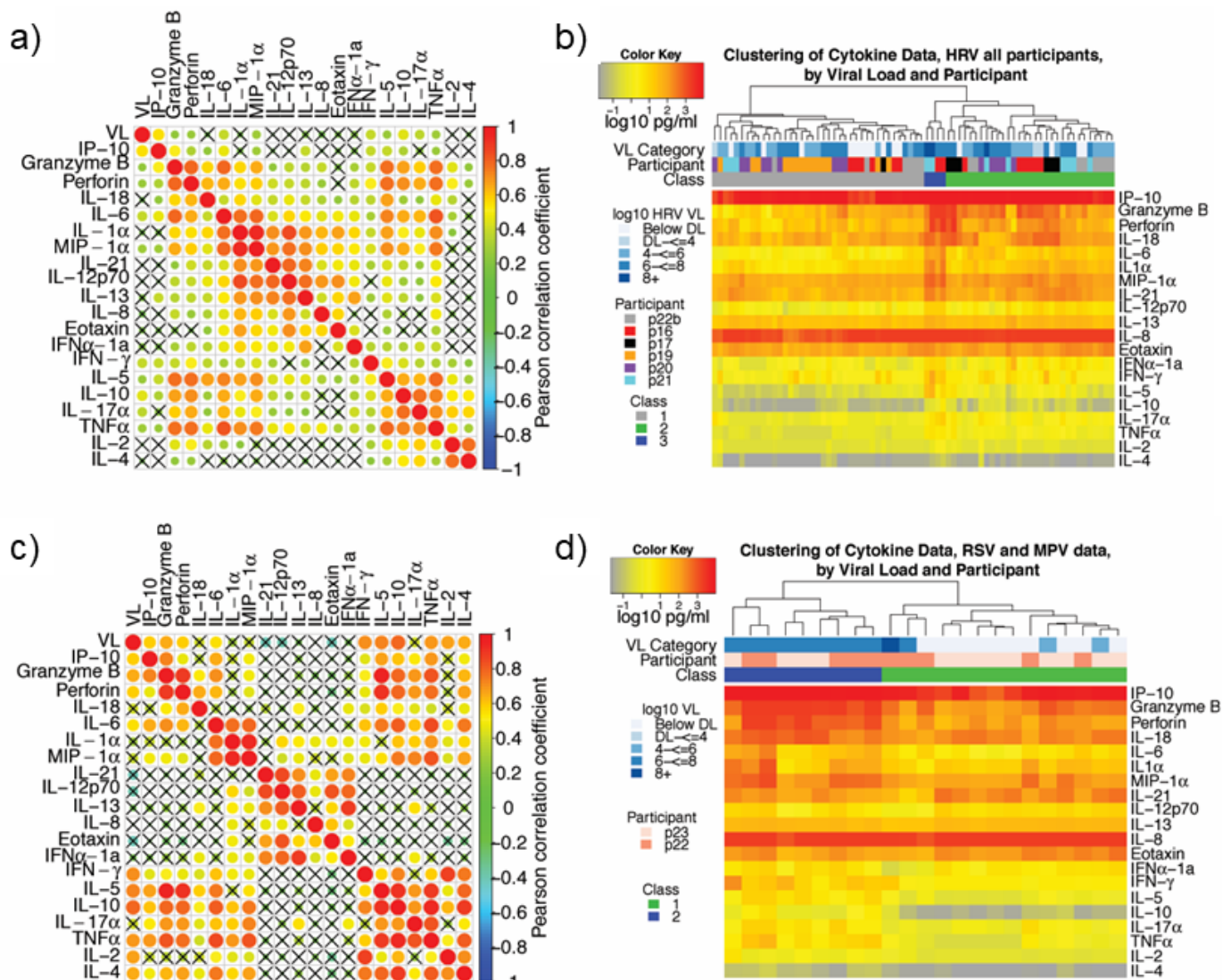
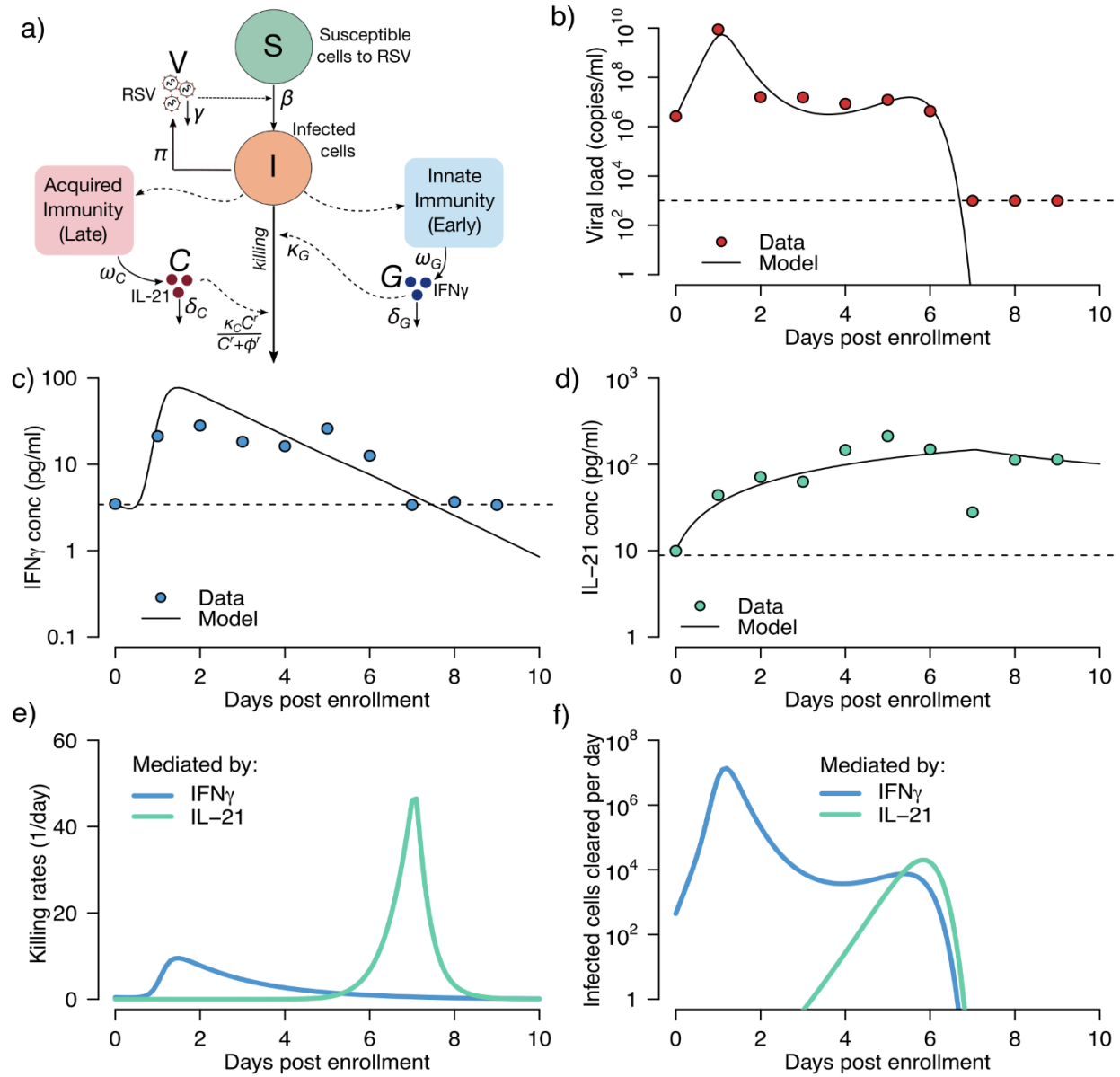


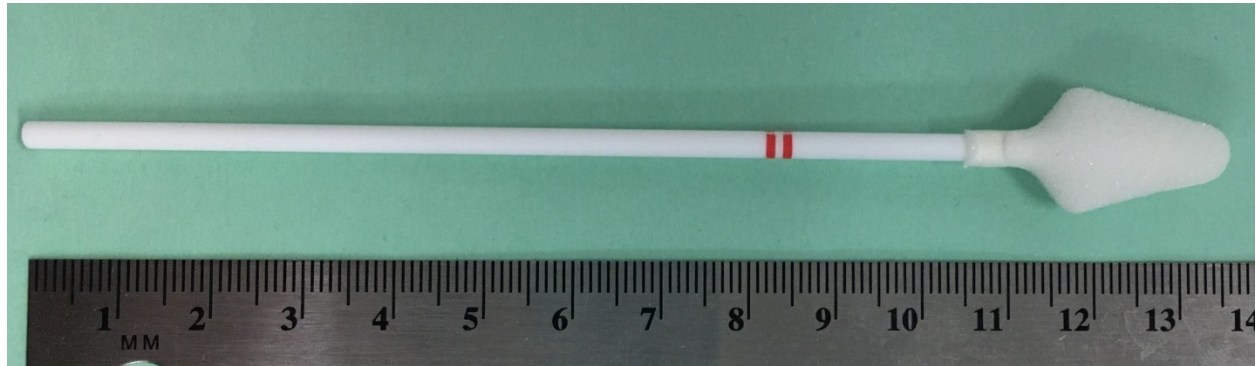
Figure 3



**Figure 4**

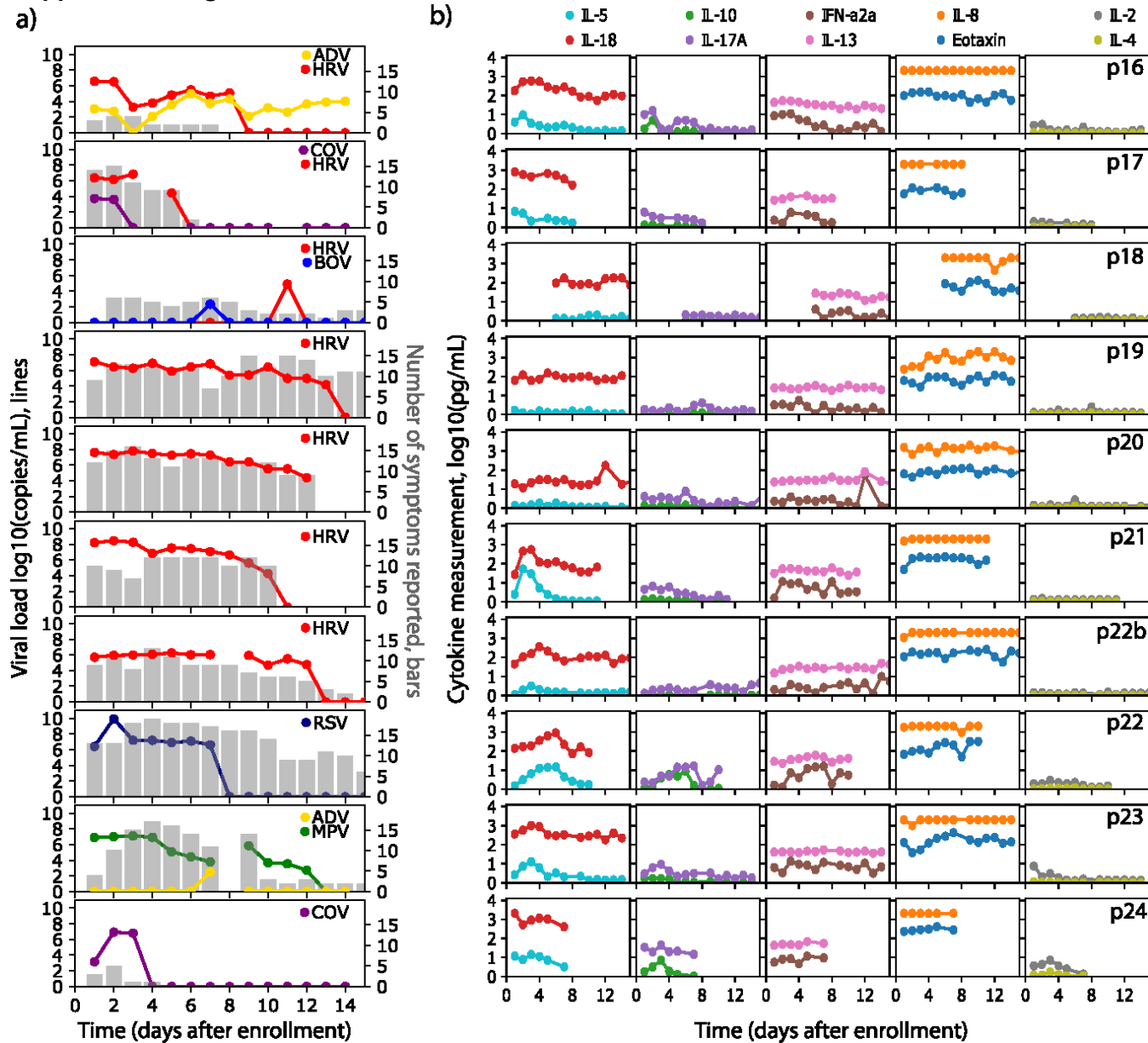


## Supplemental Figure 1



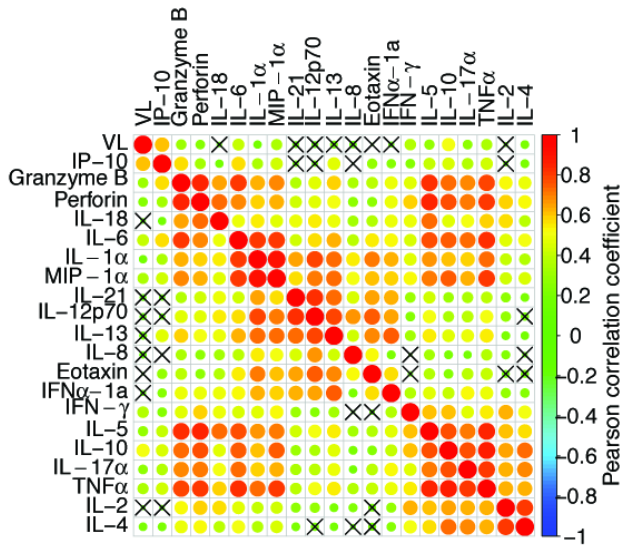


## Supplemental Figure 2

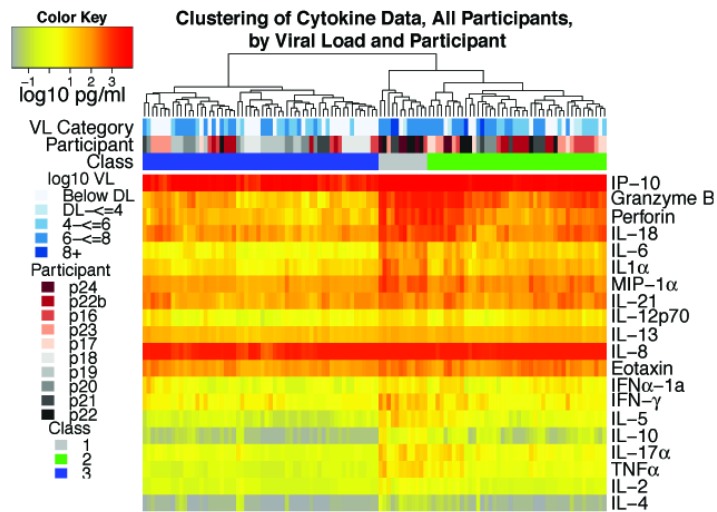


### Supplemental Figure 3

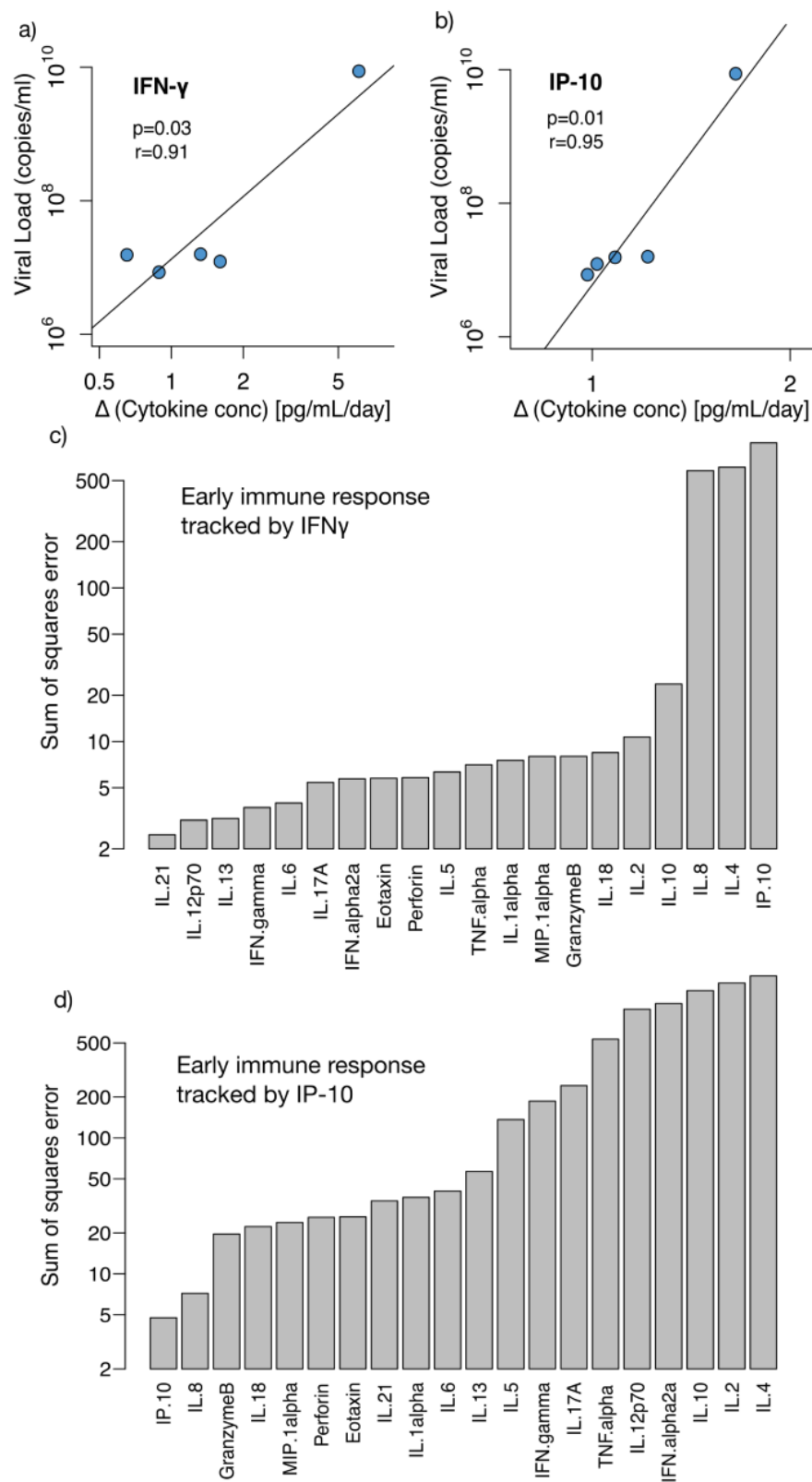
a)



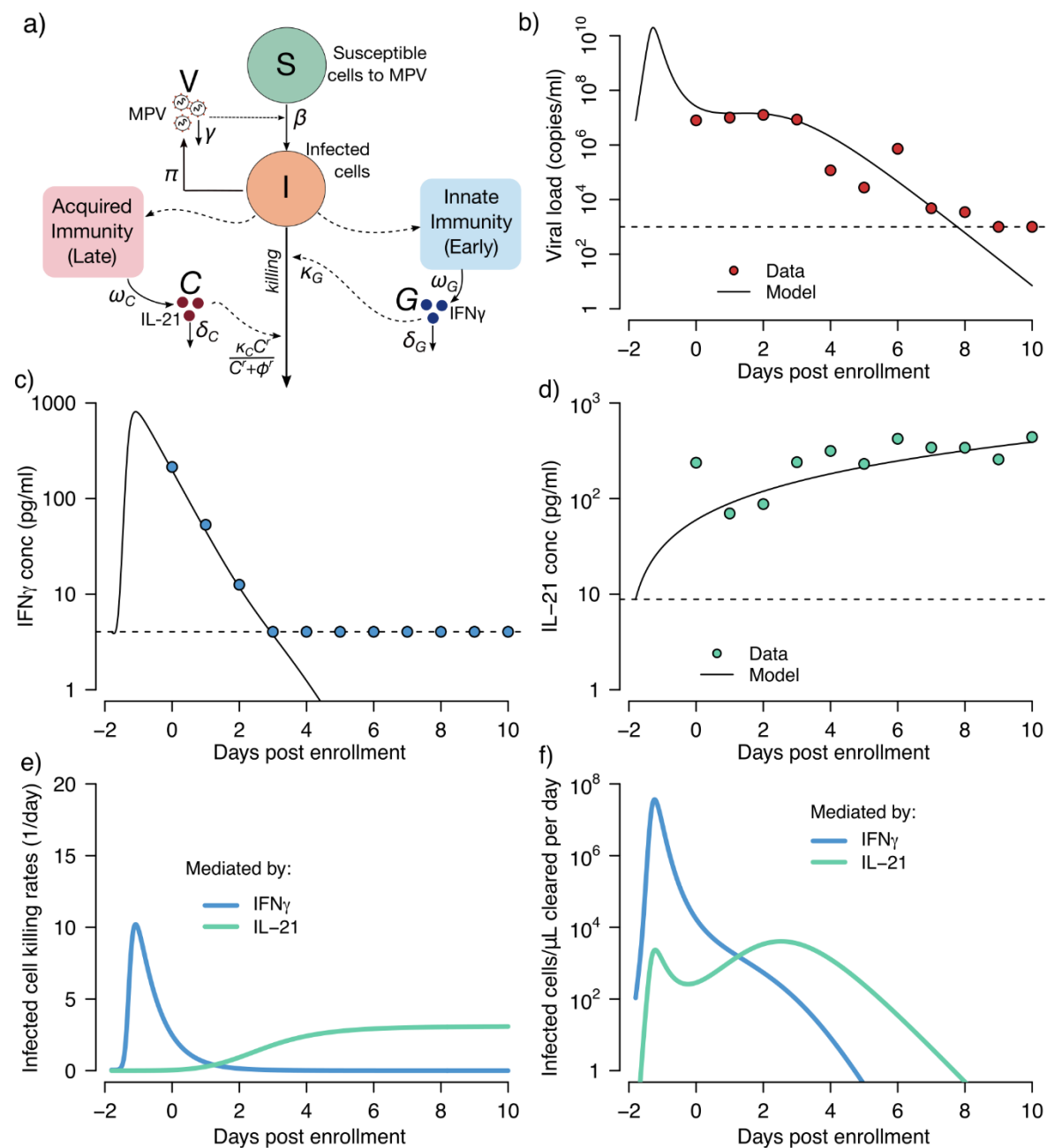
b)



## Supplemental Figure 4



## Supplemental Figure 5



**Supplemental Table 1: Symptom survey administered at enrollment (foam vs flocked swab comparison study) and daily (longitudinal sampling study).**

<b>Symptom Category</b>	<b>Specific symptom</b>
<b>Nose</b>	Runny nose
	Congestion
	Post-nasal drip
	Sinus Pain
	Sneezing
<b>Eyes</b>	Watery/burning eyes
<b>Ears</b>	Ear pain
<b>Throat</b>	Sore throat
	Hoarseness
<b>Chest</b>	Cough
	Phlegm production
	Wheezing or chest tightness
	Shortness of breath
	Chest pain
<b>Gastrointestinal</b>	Diarrhea
	Nausea
	Stomach pain
	Vomiting
<b>General</b>	Fatigue
	Fever
	Chills
	Headache
	Aching muscles
<b>Sleep Changes</b>	Sleep Disruption
<b>Sensory Changes</b>	Change in smell
	Change in taste

**Supplemental Table 2A: Foam versus foam swab concordance in left nostril.**

	Flocked Swab			
		Positive	Negative	Total
Foam Swab	Positive	4	2	6
	Negative	2	7	9
	Total	6	9	15

**Supplemental Table 2B: Foam versus foam swab concordance in right nostril.**

	Flocked Swab			
		Positive	Negative	Total
Foam Swab	Positive	5	3	8
	Negative	1	6	7
	Total	6	9	15

**Supplemental Table 2C: Foam versus foam swab concordance with results from left and right nostril combined.**

	Flocked Swab			
		Positive	Negative	Total
Foam Swab	Positive	9	5	14
	Negative	3	13	16
	Total	12	18	30

## REFERENCES

- 593 1. Dong, E., Du, H. & Gardner, L. An interactive web-based dashboard to track COVID-19  
594 in real time. *Lancet Infect Dis* (2020).
- 595 2. Onder, G., Rezza, G. & Brusaferro, S. Case-Fatality Rate and Characteristics of Patients  
596 Dying in Relation to COVID-19 in Italy. *JAMA* (2020).
- 597 3. Korean Society of Infectious, D., Korea Centers for Disease, C. & Prevention. Analysis  
598 on 54 Mortality Cases of Coronavirus Disease 2019 in the Republic of Korea from  
599 January 19 to March 10, 2020. *J Korean Med Sci* **35**, e132 (2020).
- 600 4. Patrick, G.T., *et al.* The global impact of COVID-19 and strategies for mitigation and  
601 suppression. (Imperial College London, 2020).
- 602 5. Gutierrez, P. Coronavirus mapped: which countries have the most cases and deaths? ,  
603 Vol. 2020.
- 604 6. Lipsitch, M., Swerdlow, D.L. & Finelli, L. Defining the Epidemiology of Covid-19 - Studies  
605 Needed. *N Engl J Med* **382**, 1194-1196 (2020).
- 606 7. Clark, T.W., *et al.* Viral load is strongly associated with length of stay in adults  
607 hospitalised with viral acute respiratory illness. *J Infect* **73**, 598-606 (2016).
- 608 8. Hijano, D.R., *et al.* Clinical correlation of influenza and respiratory syncytial virus load  
609 measured by digital PCR. *PLoS One* **14**, e0220908 (2019).
- 610 9. Fry, A.M., *et al.* Effects of oseltamivir treatment of index patients with influenza on  
611 secondary household illness in an urban setting in Bangladesh: secondary analysis of a  
612 randomised, placebo-controlled trial. *Lancet Infect Dis* **15**, 654-662 (2015).
- 613 10. Liu, Y., *et al.* Viral dynamics in mild and severe cases of COVID-19. *Lancet Infect Dis*  
614 (2020).

- 615 11. Agyemang, E., *et al.* Herpes simplex virus shedding rate: Surrogate outcome for genital  
616 herpes recurrence frequency and lesion rates, and phase 2 clinical trials end point for  
617 evaluating efficacy of antivirals. *J Infect Dis* **218**, 1691-1699 (2018).
- 618 12. Duke, E.R., *et al.* Viral kinetic correlates of cytomegalovirus disease and death after  
619 hematopoietic cell transplant. *Biol Blood Marrow Tr* **24**, S20-S20 (2018).
- 620 13. Green, M.L., *et al.* Cytomegalovirus viral load and mortality after haemopoietic stem cell  
621 transplantation in the era of pre-emptive therapy: a retrospective cohort study. *Lancet*  
622 *Haematol* **3**, e119-127 (2016).
- 623 14. Natori, Y., *et al.* Use of viral load as a surrogate marker in clinical studies of  
624 cytomegalovirus in solid organ transplantation: A systematic review and meta-analysis.  
625 *Clin Infect Dis* **66**, 617-631 (2018).
- 626 15. Murray, J.S., Elashoff, M.R., Iacono-Connors, L.C., Cvetkovich, T.A. & Struble, K.A. The  
627 use of plasma HIV RNA as a study endpoint in efficacy trials of antiretroviral drugs. *AIDS*  
628 **13**, 797-804 (1999).
- 629 16. Feld, J.J., *et al.* Sofosbuvir and velpatasvir for HCV genotype 1, 2, 4, 5, and 6 infection.  
630 *N Engl J Med* **373**, 2599-2607 (2015).
- 631 17. Feld, J.J., Wong, D.K. & Heathcote, E.J. Endpoints of therapy in chronic hepatitis B.  
632 *Hepatology* **49**, S96-S102 (2009).
- 633 18. Topham, D.J. & Reilly, E.C. Tissue-Resident Memory CD8(+) T Cells: From Phenotype  
634 to Function. *Front Immunol* **9**, 515 (2018).
- 635 19. Cheng, M. & Hu, S. Lung-resident gammadelta T cells and their roles in lung diseases.  
636 *Immunology* **151**, 375-384 (2017).
- 637 20. Kandasamy, M., Furlong, K., Perez, J.T., Manicassamy, S. & Manicassamy, B.  
638 Suppression of Cytotoxic T Cell Functions and Decreased Levels of Tissue Resident  
639 Memory T cell During H5N1 infection. *J Virol* (2020).



- 640 21. Smith, A.P., Moquin, D.J., Bernhauerova, V. & Smith, A.M. Influenza Virus Infection  
641 Model With Density Dependence Supports Biphasic Viral Decay. *Front Microbiol* **9**, 1554  
642 (2018).
- 643 22. Roychoudhury, P., *et al.* Tissue-resident T cell derived cytokines eliminate herpes  
644 simplex virus-2 infected cells. *J Clin Invest* (2020).
- 645 23. United States Food and Drug Administration. FAQs on Diagnostic Testing for SARS-  
646 CoV-2. Vol. 2020.
- 647 24. Campbell, A.P., *et al.* Self-collection of foam nasal swabs for respiratory virus detection  
648 by PCR among immunocompetent subjects and hematopoietic cell transplant recipients.  
649 *J Clin Microbiol* **51**, 324-327 (2013).
- 650 25. Preiksaitis, C.M., *et al.* A patient self-collection method for longitudinal monitoring of  
651 respiratory virus infection in solid organ transplant recipients. *J Clin Virol* **62**, 98-102  
652 (2015).
- 653 26. Fisher, C.E., Boeckh, M., Jerome, K.R., Englund, J. & Kuypers, J. Evaluating addition of  
654 self-collected throat swabs to nasal swabs for respiratory virus detection. *J Clin Virol*  
655 **115**, 43-46 (2019).
- 656 27. van Doremalen, N., *et al.* Aerosol and Surface Stability of SARS-CoV-2 as Compared  
657 with SARS-CoV-1. *N Engl J Med* (2020).
- 658 28. Schiffer, J.T., *et al.* Mucosal host immune response predicts the severity and duration of  
659 herpes simplex virus-2 genital tract shedding episodes. *Proc Natl Acad Sci U S A* **107**,  
660 18973-18978 (2010).
- 661 29. Antunes, K.H., *et al.* Respiratory syncytial virus reduces STAT3 phosphorylation in  
662 human memory CD8 T cells stimulated with IL-21. *Sci Rep* **9**, 17766 (2019).
- 663 30. Dodd, J.S., Clark, D., Muir, R., Korpis, C. & Openshaw, P.J. Endogenous IL-21 regulates  
664 pathogenic mucosal CD4 T-cell responses during enhanced RSV disease in mice.  
665 *Mucosal Immunol* **6**, 704-717 (2013).

- 666 31. Gassen, R.B., *et al.* RSV Downregulates IL-21/IL-21R on TFH cells via PD-L1 induction  
667 in APCS impairing protective humoral responses. 203133 (2017).
- 668 32. Kuypers, J., *et al.* Comparison of real-time PCR assays with fluorescent-antibody assays  
669 for diagnosis of respiratory virus infections in children. *J Clin Microbiol* **44**, 2382-2388  
670 (2006).
- 671 33. Lin, L.I. A concordance correlation coefficient to evaluate reproducibility. *Biometrics* **45**,  
672 255-268 (1989).
- 673 34. Hopkins, B. & Skellam, J.G. A New Method for determining the Type of Distribution of  
674 Plant Individuals. *Ann Bot*, 213-227 (1954).
- 675 35. Banerjee, A. & Dave, R.N. Validating clusters using the Hopkins statistic. in *2004 IEEE*  
676 *International Conference on Fuzzy Systems (IEEE Cat. No.04CH37542)*,, Vol. 1 149-153  
677 (Budapest, Hungary, 2004).
- 678 36. R Core Team. R: A language and environment for statistical computing. (R Foundation  
679 for Statistical Computing, Vienna, Austria, 2018).